Conformation of Peptides in Lipid Membranes Studied by X-Ray Grazing Incidence Scattering

Alexander Spaar, Christian Münster, and Tim Salditt
Department of Experimental Physics, Universität des Saarlandes, Saarbrücken, Germany

ABSTRACT Although the antimicrobial, fungal peptide alamethicin has been extensively studied, the conformation of the peptide and the interaction with lipid bilayers as well as the mechanism of channel gating are still not completely clear. As opposed to studies of the crystalline state, the polypeptide structures in the environment of fluid bilayers are difficult to probe. We have investigated the conformation of alamethicin in highly aligned stacks of model lipid membranes by synchrotron-based x-ray scattering. The (wide-angle) scattering distribution has been measured by reciprocal space mappings. A pronounced scattering signal is observed in samples of high molar peptide/lipid ratio which is distinctly different from the scattering distribution of an ideal helix in the transmembrane state. Beyond simple models of ideal helices, the data is analyzed in terms of models based on atomic coordinates from the Brookhaven Protein Data Bank, as well as from published molecular dynamics simulations. The results can be explained by assuming a wide distribution of helix tilt angles with respect to the membrane normal and a partial insertion of the N-terminus into the membrane.

INTRODUCTION

Transmembrane helices are the predominant structural element of membrane-spanning domains of polypeptides associated with the lipid bilayer. Apart from membrane proteins, many short peptides are known to adopt a helical conformation at the lipid bilayers. Tilt angles of the helical axis, rotation angle around this axis, degree of helicity, and the interaction and association of several helices are important parameters and structural aspects, providing a basis for many biological functions. Therefore, structural methods are required to probe polypeptide assemblies in and at the lipid bilayer. To this end, diffraction from highly aligned, multilamellar samples can be used as a sensitive probe for lipid-peptide interaction.

Amphiphilic peptides are an important and relatively simple class of membrane-active polypeptides with a number of different functions in the innate host-defense system of many organisms, which require improved structural characterization. Due to the structural simplicity, these peptides may also serve as a testing ground for experimental techniques. Reviews on amphiphilic and antimicrobial peptides, are provided by Bechinger (1997, 1999), Biggin and Sansom (1999), Huang (2000), Marsh (1996), Matsuzaki (1999), Shai (1999), and Sitaram and Nagaraj (1999). Well-known examples are ceropins expressed in insects, or magainin, the first antimicrobial peptide discovered in vertebrates. Magainin is expressed in the intestines and the skin of the frog *Xenopus laevis*. Host-defense and cytolytic peptides are amphiphilic polypeptides of typically in-between 20 and 40 amino acid residues, with well-defined secondary structures formed by the interaction with the lipid bilayer. It has been shown that antimicrobial peptides interact directly with the microbial cell membranes rather than with specific membrane proteins, subsequently causing an increase in membrane permeability and cell lysis. Other examples of seemingly similar peptides are cytolytic to mammalian cells, like the well-known alamethicin of the fungus *Trichoderma viride*. However, despite recent advances stemming from a large number of different techniques, most structural models remain incomplete or partially hypothetical and necessitate in-depth structural characterization. To this end, a refinement of scattering techniques including sample preparation, measurement, and data analysis is needed. In this article, we report an x-ray scattering study on aligned lipid membranes at different molar peptide/lipid-concentrations of alamethicin. We evaluate the wide-angle scattering distribution measured in a two-dimensional mapping of reciprocal space as a function of momentum transfer parallel $q_{||}$ and perpendicular q_z to the oriented lipid bilayers.

Alamethicin is a 20-amino-acid peptide from the fungus *T. viride*, reviewed in Bechinger (1997, 1999), Cafiso (1994), Kessel and Ben-Tal (2002), and Sansom (1993). Together with hypelcins, trichorzianins, and zervamicins it belongs to a class called peptaibols (Duclohier and Wrblewski, 2001; Sansom, 1993), which have similar structure and are also known to exhibit channel activity. Alamethicin is rich in hydrophobic amino acids, in particular α-methylalanine (Ala) and in the amino acid α-aminoisobutyric acid (Aib), which supports the helical conformation. The sequence is Ac-Aib-Pro-Aib-Ala-Aib-Ala-Gln-Aib-Val-Aib-Gly-Leu-Aib-Pro-Val-Aib-Aib-Glu-Gln-Phl-OH. The crystal structure of alamethicin was solved over 20 years ago by Fox and

Submitted January 23, 2004, and accepted for publication March 31, 2004.

Address reprint requests to Tim Salditt, E-mail: tsaldit@gwdg.de.

Alexander Spaar's present address is Center of Bioinformatics, Universität des Saarlandes, Im Stadtwald, D-66041 Saarbrücken, Germany.

Tim Salditt's present address is Institute for X-Ray Physics, University of Göttingen, Geiststr. 11, D-37073 Göttingen, Germany.

0006-3495/04/07/396/12 $2.00

doi: 10.1529/biophysj.104.040667

Richards by x-ray crystallography (Fox and Richards, 1982). In helical conformation the length of the molecule is 33 Å; the Pro^{14} residue acts as a bend in the helix.

Alamethicin has been extensively studied using a large variety of techniques. The peptide binds strongly to lipid bilayers and forms voltage-dependent, mildly cation-selective channels (Aguilella and Bezrukov, 2001; Boheim, 1974; Hall, 1981; Schwarz and Savko, 1982; Vodyanoy et al., 1983), which act as rectifiers (Woolley et al., 1997). It inserts via its N-terminus in response to an external voltage. However, the mechanism for the channel gating is not completely clear. The dipole moment of ~75 Debye = 16 eÅ (Schwarz and Savko, 1982) corresponds to a net +1/2 charge at the N- and a −1/2 charge at the C-terminus of the helix. Many experiments suggest that alamethicin assumes transmembrane orientation, with its N-terminus partially buried in the hydrophobic region of the lipid chains, whereas the C-terminus is supposed to be hydrogen-bonded to the water or the lipid headgroups (Galaktionov and Marshall, 1993; Jayasinghe et al., 1998; Kessel et al., 2000a,b; Tieleman et al., 1999a,c). The channel activity occurs in discrete, multilevel conductances. This supports the barrel-stave model for the channel structure in which the discrete conductance steps result from a varying number of pore-forming peptides (Baumann and Mueller, 1974; Boheim, 1974; Boheim et al., 1983; Ehrenstein and Lecar, 1977). The open alamethicin pore has been suggested to consist of 3–11 parallel helical molecules arranged around a water-filled pore, depending on the hydration and the lipid (Cantor, 2002; He et al., 1996a). Alamethicin in lipid bilayers has also been extensively studied by molecular dynamics (MD) simulations (Biggin et al., 1997; La Rocca et al., 1999; Tieleman et al., 1999c, 2001). Tieleman and co-workers studied alamethicin pores by MD simulation, whereas the most stable model was found to be the hexamer (Tieleman et al., 1999b, 2002). In DLPC the size of the pores corresponds to ~8–9 monomers with a water pore of ~18 Å in diameter, as inferred from a pore-pore correlation peak in small-angle neutron scattering (Yang et al., 1999). NMR studies showed that in DMPC membranes alamethicin in the transmembrane configuration is tilted by 10–20° to match the hydrophobic thickness of the bilayer (Bak et al., 2001). However, the detailed structure of the channel is still under debate (Bven et al., 1999; Ionov et al., 2000), and the majority of peptides is not always in the oligomeric channel state. In fact, the conformation of peptides in lipid membranes was found to be very sensitive to environmental parameters like the temperature, humidity, and peptide/lipid-concentration (*P/L*). NMR studies showed that the degree of helicity in the presence of lipid bilayers depends on the physical state of the lipid (i.e., *P/L*) and the presence of transmembrane potentials (Bechinger, 1997). By oriented circular dichroism and x-ray diffraction experiments, He et al. (1996b) demonstrated that up to a critical lipid/peptide ratio which is lipid-dependent, alamethicin adsorbs on the membrane surface, resulting in a thinning of the membrane. At a concentration of $P/L = 1/15$ or higher all peptides adopt the transmembrane state. Circular dichroism spectroscopy experiments on alamethicin in DOPC membranes have shown that at lower temperatures alamethicin forms membrane-spanning channels whereas monomeric states are favored at higher temperatures (Woolley and Wallace, 1993). With increasing temperature the helix starts to partially unfold. Since the Ala residues stabilize the helical structure, the N-terminus is more stable than the C-terminus (Yee et al., 1997).

In summary, a wealth of information is available for the well-studied peptide alamethicin, making it an ideal system for development and refinement of novel techniques to elucidate the structure of membrane polypeptides. At the same time the shortcomings of state-of-the-art techniques to probe membrane proteins and peptides are also obvious. The helical conformation is in most cases assessed only indirectly, from conductance or absorption spectroscopy, as opposed to a direct structural probe. Simple parameters such as the helix length, tilt, pitch, or the number of helices in an oligomeric pore are difficult to assess. Here we address the question whether wide-angle scattering in form of reciprocal space mappings (RSMs) on highly oriented stacks of bilayers can overcome some of these limitations. In particular we investigate the intrinsic scattering signal of peptides directly, and independently from the aggregation state or in-plane ordering of helices. Thus, here we are primarily interested in the helix scattering signal, rather than the small-angle scattering patterns, which can evidence the correlation of pores or parameters of bilayer density profile.

To our knowledge, the helical scattering distribution of alamethicin has not been measured before. In this study we found a surprisingly strong signal which is distinctly different from the simulated scattering distribution of an ideal helix in the transmembrane state.

MATERIALS AND METHODS

The lipids 1,2-dilauroyl-*sn*-glycero-3-phosphatidylcholine (DLPC) and 1-oleoyl-2-palmitoyl-*sn*-glycero-3-phosphatidylcholine (OPPC) were purchased from Avanti Polar Lipids (Birmingham, AL) with a purity >99%, and alamethicin was bought from Sigma Aldrich (St. Louis, MO) with a purity >98.9%. Both lipids and peptides were used without further purification. Initially they were separately weighed and dissolved in isopropanol at a concentration of 20 mg/ml for the lipids and 1.5 mg/ml for the peptides. The lipid and peptide solutions were mixed with the specified molar *P/L*, and spread onto silicon substrates (111-orientation, 1" diameter), following essentially the procedure described by Seul and Sammon (1990). The wafers were cleaned by subsequent washing in methanol, and made hydrophilic in a plasma cleaner for approximately half a minute. Between each step the wafers were thoroughly rinsed with ultrapure water (specific resistance ≥ 18 MΩ cm, Millipore, Bedford, MA). A drop of 0.2 ml was then carefully spread onto the substrate which was placed on a spin coater. The angular velocity was chosen to be 230 rpm, fast enough for aligning the membranes, preventing film rupture, and dewetting but also slow enough to keep the whole solvent on the wafer (Mennicke and Salditt, 2002). After 10 min the sample was dried, yielding a very uniform

film. Remaining traces of solvent in the sample were removed by exposing the samples to high vacuum over 24 h. The films were then rehydrated in a hydration chamber, forming a highly oriented stack of several thousand membranes.

The samples have been characterized separately, but under the same conditions as in the experiment where the RSMs have been measured. The membrane periodicity d was almost constant with varying peptide concentration. For the pure lipids at $P/L = 0$, $d = 45.0$ Å for DLPC and $d = 51.8$ Å for OPPC, reflecting the different chain length of the two lipids. At $P/L = 1{:}100$, $d = 44.6$ Å was obtained for the DLPC sample, $d = 52.0$ Å for the OPPC sample, at $P/L = 1{:}25$, $d = 45.3$ Å for the DLPC sample, and $d = 52.2$ Å for the OPPC one. The orientational alignment of the multilamellar stack with respect to the substrate (mosaicity) was typically on the order of a few hundreds of degrees. Whereas this is well known to be achieved for pure lipid bilayers (Spaar and Salditt, 2003), we found that the low mosaicity is preserved also at high P/L, even though the positional correlations along z between the bilayers decrease with P/L. The low mosaicity is evidenced in three different ways: 1), measurement of reflectivity curves and observation of a critical angle for total external reflection; 2), rocking curves; and 3), images of the lamellar peaks obtained on the two-dimensional detector in the forward direction, which show that the diffuse scattering at the Bragg positions is not curved as would be the case for samples of high mosaicity. A mosaicity lower than the critical angle which is on the order of 0.1° (depending on wavelength and sample density) is a prerequisite to apply interface-sensitive x-ray scattering techniques for structural studies of solid-supported bilayers.

Sample environment

During the x-ray experiments, the solid-supported multilamellar films were kept in a closed temperature-controlled chamber. The chamber consists of two concentric aluminum cylinders, with kapton windows. The inner cylinder was kept at a constant temperature of $T = 45^{\circ}$ C by a flow of oil, connected to a temperature-controlled reservoir (Julabo, Seelbach, Germany) with PID-control. The space between the two cylinders was evacuated to minimize heat conduction. The temperature was measured close to the sample holder by a Pt100 sensor, indicating a thermal stability >0.02 K over several hours. At the bottom of the inner cylinder a water reservoir was filled with salt-free Millipore water (Millipore, Billerica, MA), such that the sample was facing a vapor phase of nominally 100% relative humidity. Despite the nominally full hydration condition, DMPC bilayers were only partially swollen with repeat distance of typically $d \simeq 50$ Å in the fluid L_{α}-phase, i.e., they were only partially hydrated. This limited swelling of solid-supported lipid films is well known as the so-called vapor-pressure paradox (Podgornik and Parsegian, 1997), and can only be circumvented in chambers of special design (Nagle and Katsaras, 1999).

X-ray experiment

The samples were characterized by x-ray reflectivity at the bending magnet beamline D4 of the DORIS storage ring at HASYLAB/DESY using photon energy of 20 keV. The reciprocal space mappings (RSMs) have also in part been carried out at D4, using a fast scintillation counter (Cyberstar, Oxford-Danfysik, Oxford, UK). The data has been collected using two-dimensional mesh scans (TASCOM diffractometer control software, HASYLAB, Hamburg, Germany) and an exit angle collimation distance, defined by detector and guard slits, leading to high signal/noise ratios. The typical accumulation time of a mesh scan RSM is between 10 and 20 h, depending on the desired resolution and/or counting statistics. Much faster data accumulation can be realized by using two-dimensional detectors like the charge-coupled device (CCD) camera—but at the price of higher background levels. Additional RSMs were measured using a CCD detector (Princeton CCD, 1242×1152 pixel, Princeton Instruments, Roper Scientific, Ottobrunn, Germany) at the undulator beamline ID1 of the European Synchrotron Radiation Source (Grenoble, France), again with a photon energy of 20 keV, set by a double-bounce Si(111) monochromator. Compared to smaller energies $E < 20$ keV, the ratio of the scattering cross-section to the photoabsorption cross-section is significantly higher at 20 keV, so that radiation damage is minimized. Note, however, that long sample illumination by the undulator beam led to changes induced by radiation damage. Therefore, long mesh scans were avoided, and replaced by a combination of short CCD exposures (on the order of seconds to minutes). Whereas the undulator also performs well at $E > 20$ keV, the CCD detector sensitivity is expected to decrease with E. A further issue to optimize is the Compton background, which can become important for low Z samples at high photon energy E. Test experiments have been performed at photon energies of 70 keV (BW5 beamline at HASYLAB) to map out the complete reciprocal space (including the small- and wide-angle regions) on a single CCD frame.

For the undulator experiment at the ID1 beamline of the European Synchrotron Radiation Source, the CCD was mounted on the detector arm of the six-circle diffractometer. The pixel positions on the camera correspond to diffraction angles $\alpha = \alpha_i + \alpha_f$ (in the plane of incidence) and 2θ (out of the plane of incidence); see Fig. 1. From these angles, the different components of the wave vector (momentum transfer) can be calculated as

$$q_x = \frac{2\pi}{\lambda}(\cos\alpha_f \cos(2\theta) - \cos\alpha_i),$$
$$q_y = \frac{2\pi}{\lambda}\cos\alpha_f \sin(2\theta),$$
$$q_z = \frac{2\pi}{\lambda}(\sin\alpha_i + \sin\alpha_f).$$

A wide range of reciprocal space was then mapped by moving the camera to well-chosen positions, taking a set of five exposures with partial overlap, each with an acquisition time of 100 s and 300 s. By combining these five exposures we got an image of the reciprocal space (see Fig. 7 *A*; see also Spaar and Salditt, 2003). The direct beam was blocked by lead tape at the side of the camera. The angle of incidence was chosen to optimize scattering volume, and to minimize background from the substrate (penetration depth). At the same time, a strong specular reflection has to be avoided. For the example given in Fig. 7 *A*, the incidence angle was $\alpha_i = 0.5^{\circ}$ for all exposures, except for the one in the forward direction showing the strong diffuse Bragg sheets, which has been measured at $\alpha_i = 1^{\circ}$ to avoid detector saturation. At these small angles the momentum transfer in the direction of the primary beam q_x is always dominated by q_y, even at high q_z, except for very small q_y around the incidence plane—not considered here. Therefore it is an excellent approximation to set $q_{\parallel} = \sqrt{q_x^2 + q_y^2} \simeq q_y$ for almost the total range of the RSM (Salditt et al., 1995), in particular in the vicinity of the chain correlation peak. In this approximation, the vertical and parallel components of the momentum transfer are orthogonal.

Importantly, a beam flux at the sample on the order of 10^{11} photons per second as obtained by vertical and horizontal focusing at ID1 led to radiation-induced shifts in the diffraction intensity after ~60 min, a time which is too short for the positioning of a point detector during a two-dimensional mesh scan. Contrarily, the use of the CCD cut down the acquisition time below the threshold for observable radiation damage. The absence of radiation damage has been cross-checked by translating the sample through the beam, sized 0.5 mm (horizontal) × 0.2 mm (vertical).

THE HELICAL DIFFRACTION PATTERN: ANALYTICAL EXPRESSION AND THEORY

The diffraction pattern of an ideal helix as first written down by Pauling and Corey (1951) was a milestone in structural biology. It can be regarded as the

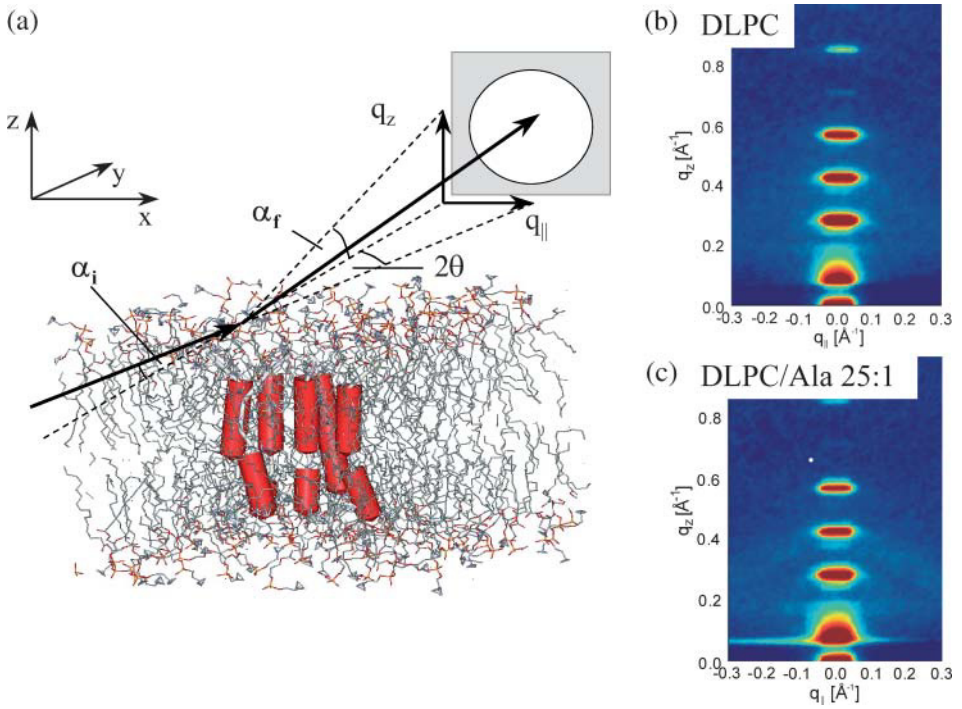

FIGURE 1 (*a*) Sketch combining the MD data set (Tieleman et al., 2002) and the scattering geometry used. The lipids are displayed as sticks, the alamethicin helices are schematically shown as tubes. The momentum transfer vertical to the membrane plane q_z is controlled by the scattering angle $\alpha_i + \alpha_f$, the lateral momentum transfer $q_{||}$ mainly by $2\,\theta$. (*b* and *c*) The lamellar peaks measured in the forward direction (photon energy 70 keV, BW5 beamline HASYLAB, MAR image plate detector, logarithmic color code), for a sample of pure DLPC, and of high peptide concentration, $P/L = 1{:}25$, in the fluid L_α phase. The fact that the peaks are not curved around an arc indicates the high degree of orientation, which is obtained for pure lipids was well as for lipid/peptide mixtures.

form factor of an ideal helical molecule, i.e., as an intramolecular scattering signal with positional correlation arising from bond length, angles, and macromolecular folding. The periodic structure of a helix in the direction along the helical axis z gives rise to a pronounced maximum in the diffraction pattern, the so-called helix peak at $q_z \sim 1.1$ Å^{-1} and $q_{||} \sim 0.65$ Å^{-1}. These values depend only on the helix pitch P and radius R_h and are characteristic for the α-helix. From the width of the peak in q_z-direction the number of helical turns and therefore the helix length can be determined. Higher order peaks and side oscillations are typically not observed since they are smeared out by positional fluctuations. Note that in this section we mostly consider the form factor $F(q_z, q_{||})$ to be a function of vertical q_z and parallel $q_{||} = \sqrt{q_x^2 + q_y^2}$ only, since we assume in-plane isotropy (rotational averaging); see also Fig. 1 for the coordinate system. In the following, we calculate the form factor of an ideal helix as well as of a pore constructed from several parallel helices arranged on a regular polygon, aiming at a simple model for a transmembrane pore. Since amphiphilic transmembrane peptides tend to aggregate and to form pores, we investigate the effect of pore formation on the scattering distribution, i.e., we investigate the structure factor of the pore in reciprocal space. Note that in the literature a barrel-stave structure is reported for alamethicin in the inserted (transmembrane) state (He et al., 1996b), whereas magainin 2 is believed to form a toroidal pore structure (Matsuzaki, 1998; Ludtke et al., 1996). The analytical expressions are then compared to numerical results, taking into account the full molecular coordinates. The molecular coordinates are taken from 1), the x-ray crystallography structures as deposited in the Brookhaven Protein Data Bank, and 2), published MD simulation results by Tieleman et al. (1999a, 2002). It turns out that for nonideal (real) helices the helix peak is shifted to smaller $q_{||}$-values because of a helix bending and the scattering contribution of the side chains. The form factor of alamethicin at different tilt angles has been computed to get information about the distribution of helix tilt angles from experimentally obtained scattering patterns. The interplay between the molecular form factor and the structure factor of the pore is investigated analytically and numerically. The structure factor leads to additional oscillations in the $q_{||}$-direction. However, it is not clear whether these oscillations can be detected experimentally. Based on the analysis presented here, the measured diffraction patterns will be discussed in the next section.

Form factor of ideal helices

To get information about the relationship between the helix parameters and the position and width of the helix peak, the alamethicin molecule is approximated by an ideal helix. For the calculation, the z axis is defined as the direction of the helix axis. The helix parameters are the number of atoms N_h, the radius R_h, the pitch P, and the number of atoms per pitch n_p. The structure factor can be calculated analytically and written as a sum of Bessel functions (see Appendix):

$$F_{\text{helix}}(q_{||}, q_z) = 1 + 2\sum_{\Delta n=1}^{N_h-1}\left(1 - \frac{\Delta n}{N_h}\right) \times \cos\frac{q_z \Delta n P}{n_p} J_0\left(2\, q_{||}\, R_h \sin\frac{\Delta n \pi}{n_p}\right). \quad (1)$$

From this expression the position of the helix peak is derived as

$$q_{||} = \frac{5\pi}{8R_h}, \quad q_z = \frac{2\pi}{P}, \quad (2)$$

which in Fig. 2 *A* is marked by dashed lines. The peak width in q_z-direction is inversely proportional to the total length of $L_h = N_h\, P/n_p$:

$$\Delta q_z \simeq \frac{5.57}{N_h\, \Delta h} = \frac{5.57}{L_h} \quad \text{(FWHM)}. \quad (3)$$

The number of helix turns n_t can therefore be written as the ratio of the peak position and the peak width:

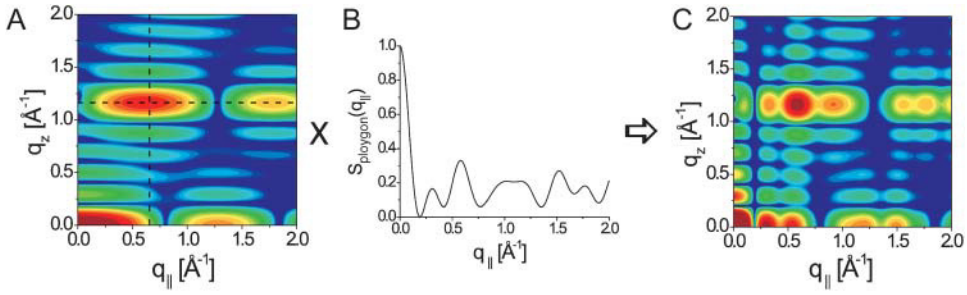

FIGURE 2 Illustration of Eq. 5 for the calculation of the structure factor of a pore of six helices. (*A*) The structure factor of an ideal helix; the dashed lines indicate the peak position, as derived from Eq. 2. (*B*) The structure factor of a polygon with six vertices is displayed. (*C*) The resulting structure factor of a helix pore.

$$n_t \simeq \frac{5.57\, q_z}{2\pi\, \Delta q_z} \simeq 0.886 \frac{q_z}{\Delta q_z}. \quad (4)$$

Fig. 2 *A* displays the form factor (Eq. 1) of an α-helix with radius $R_h = 3$ Å, pitch $P = 5.4$ Å, $n_p = 3.6 \times 3$ atoms per pitch, and $N_h = 60$ atoms as a model for alamethicin (three backbone atoms are considered per residue). Pronounced oscillations in q_z- and in $q_\parallel$-direction and two intense peaks are observed: the helix peak at $q_z = 1.16$ Å^{-1}, $q_\parallel = 0.65$ Å^{-1}, and a peak in the forward direction at $q = 0$, broadened with respect to experimentally observed primary beam by finite size.

We now turn to the construction of simple models for a transmembrane pore consisting of N_p identical peptides. As in the previous section the structure factor is first calculated analytically with the simplified assumption of ideal helices. The pore is constructed from parallel helices which are arranged on a regular polygon. Note that in a pore of amphipathic peptides the helices are arranged in such a way that the polar faces point inwards and the hydrophobic faces outwards, i.e., the peptides are rotated around the helix axis by an angle of $2\pi/N_p$ with respect to the neighbored molecules. For simplicity this effect is not considered in the following calculation. By defining a single helix as the basis and the polygon as the lattice, as usual in crystallography, the scattering of the helix pore is calculated by multiplying the Fourier transform of the helix (helical form factor), with the Fourier transform of the polygon (structure factor):

$$S_{pore} = F_{helix} \times S_{polygon}. \quad (5)$$

The value $S_{polygon}$ is calculated by Fourier transformation of a regular polygon with N_p vertices and the radius R_p. The z axis is again defined as the direction of the helix axis, whereas the polygon is arranged in the x,y plane. Because of the orientation of the polygon, the structure factor is only a function of $q_\parallel$. The calculation is similar to that of the structure factor of an ideal helix, and it can also be written in terms of Bessel functions:

$$S_{polygon}(q_\parallel) = 1 + 2\sum_{m=1}^{N_p}\left(1 - \frac{m}{N_p}\right) J_0\left(2\, q_\parallel R_p \sin\frac{m\pi}{N_p}\right). \quad (6)$$

In Fig. 2 *B* the structure factors of a polygon with radius $R_p = 12.5$ Å and $N_p = 6$ vertices is displayed. It shows rather irregular oscillations stemming from the Bessel functions and reflecting the N_p-symmetry of the pore. Fig. 2 *C* shows the structure factor of a pore with $N_p = 6$ and peptide-to-peptide distance of $R_p = 12.5$ Å helices, which has been calculated according to Eq. 5.

Form factor of alamethicin

For the comparison with the experimental diffraction pattern, the form factor of alamethicin as calculated for realistic atomic coordinates seems to be a more appropriate model than the assumption of an ideal helix. The coordinate file is taken from the Protein Data Bank (PDB code 1AMT; http://www.rcsb.org/pdb); the structure has been obtained by a x-ray crystallography study (Fox and Richards, 1982). Note that in this study three different helical structures of alamethicin were found to co-crystallize. We therefore have computed the form factor for the three helical structures separately, followed by an average over the three individual results. In Fig. 3 the form factor of alamethicin is displayed (Fig. 3 *A*) in the transmembrane state and (Fig. 3 *B*) adsorbed on the membrane surface, again after rotational averaging in the x,y plane as discussed above. The helix peak in Fig. 3 *A* is located at $q_\parallel = 0.64$ Å^{-1} and $q_z = 1.09$ Å^{-1}. In the parallel conformation (surface, i.e., *S*, state according to the notation of Huang and co-workers), the peak is observed with interchanged $q_\parallel$- and q_z-positions. Moreover, the peak intensity is much lower because of the averaging in azimuthal direction. According to Eq. 2 derived for the ideal helix, the position of the helix peak corresponds to a helical pitch of 5.76 Å and a radius of $R_h = 3.07$ Å. Although the pitch corresponds well to the value of $P_h = 5.7$ Å obtained from the (real space) coordinate files, the radius of the coordinate files is significantly smaller—$R_h = 2.5$ Å. This can be explained on the basis of the side-chain contributions. As shown in Münster et al. (2002), a bending of the helix axis as well as additional atoms which are not positioned on the helix lead to a shift of the helix peak to smaller $q_\parallel$-values. The width of the helix peak along q_z (at $q_\parallel = 0.64$ Å^{-1} in Fig. 3 *A*) is found to be 0.17 Å^{-1} (full width at half-maximum, i.e., FWHM, Gaussian fit), yielding a helical length of $l_h = 32.8$ Å from Eq. 3 or equivalently 5.7 helical turns. This has to be compared to 4.9 helical turns inferred from the coordinate file. Note that the first 13 residues in the coordinate file of alamethicin are helical, and that in this region the three helical structures are very similar. The overall length of the molecule is 33.9 Å, whereas the helical backbone is extended over ~28 Å. From the comparison it can be concluded that the q_z-position is very well reproduced by Eq. 2, whereas the formula of the $q_\parallel$-position must be regarded with caution. Also the helical length and therefore the number of turns is overestimated by using the simple formula for an ideal helix.

We now turn again to the pore constructed from several identical peptides, but this time using the molecular coordinates rather than the ideal helix. The pore was constructed with MATLAB such that the polar faces point to the pore center. Fig. 3 *C* shows the top view of a pore with six alamethicin molecules and the corresponding structure factor. Note that the intensity pattern indeed shows some resemblance with the analytical result for the ideal helix pore shown in Fig. 2 *C*. The oscillations in $q_\parallel$-direction reflecting the hexagonal symmetry of the pore are clearly visible in both images. It is presumed that more realistic models of peptide pores are provided by molecular dynamics simulations. Tieleman and co-workers performed simulations of alamethicin channels with 4–8 peptides in a POPC bilayer and surrounding water (Tieleman et al., 1999b, 2002). For the comparison, the structure factor has been computed from the simulation with six alamethicins and 102 POPC molecules by Fourier transformation. In Fig. 4 *A* the top view of the channel according to Tieleman and co-workers are displayed for illustration; see also Fig. 1. The peptide-to-peptide distance is ~11 Å. Fig. 4 *B* shows the structure factor of the coordinate set with both peptide and lipid contributions, whereas Fig. 4 *C* shows only the con-

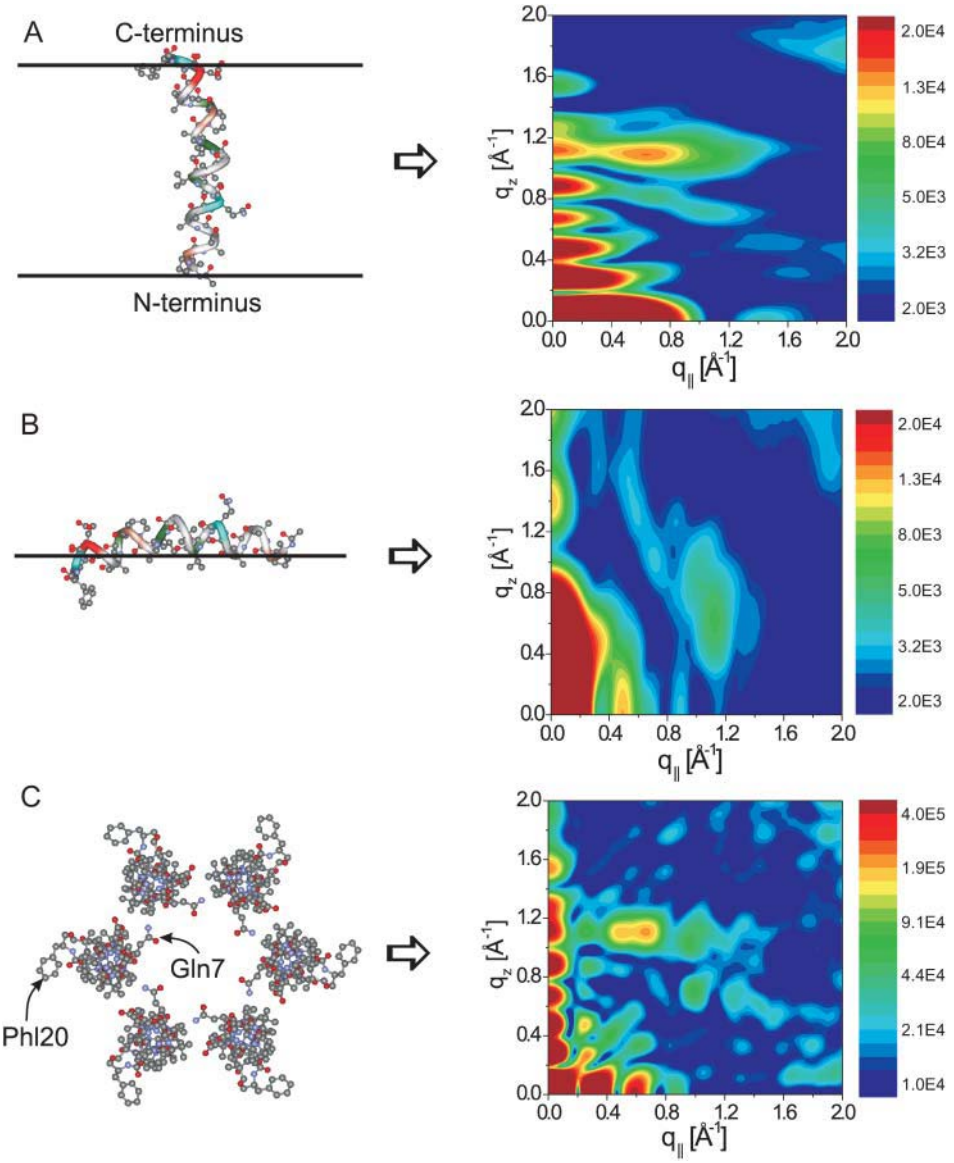

FIGURE 3 Schematic illustration of alamethicin (*A*) in transmembrane orientation and (*B*) adsorbed on the surface together with the logarithmic plots of the corresponding structure factors. (*C*) The construction of a pore of six alamethicins with a peptide-to-peptide distance of 12.5 Å together with a logarithmic plot of the structure factor.

tribution of the alamethicin molecules. In the structure factor of the six peptides (Fig. 4 *C*) the helix peak is clearly visible. The q_z-position of 1.17 Å^{-1} indicates an average helix pitch of 5.4 Å. The additional oscillation in $q_{||}$-direction, however, is weaker because of a loss in hexagonal order compared to the constructed pore. Note that in Fig. 4 *B* the chain correlation peak is more intense than the helix peak. The oscillation stemming from the pore formation is smeared out and is almost unobservable.

The comparison demonstrates that a loss of the strong pore symmetry already leads to a smearing of the oscillations in the direction of $q_{||}$. In experiments, the oscillatory pattern will be additionally averaged out due to thermal fluctuations of both the membranes and the peptides and also a possible distribution of pore sizes or number of peptides in the pores. The presence of pores as well as their (averaged) radius and the number of peptides is therefore probably not detectable experimentally by the evaluation of the helical scattering distribution. Alternative routes to get information about the pore structure rely on the scattering signal of the pores in the small-angle region, i.e., by small-angle neutron scattering (Yang et al., 1999), or the detailed analysis of the diffraction peaks stemming from the crystallization of the peptide pores (Yang et al., 2000).

THE HELICAL DIFFRACTION PATTERN: EXPERIMENTAL RESULTS

In a previous x-ray scattering experiment on the transmembrane peptide gramicidin D (in DMPC and DLPC membranes), a helical pitch of 4.7 Å was reported (Katsaras et al., 1992). The pitch of the magainin 2 helix in DMPC membranes was found to be even smaller, 4.5 Å (Münster et al., 2002). In experiments on purple membranes with bacteriorhodopsin a pitch of 4.9 Å was measured. The increasing width of the helix peak with increasing temperature was monitored and used as evidence for partial thermal unfolding of the α-helices (Müller et al., 2000). All reported values for the helix pitch in the transmembrane state seem, however, quite small compared with the pitch of 5.4 Å for a free α-helix, indicating a compression of the helices due

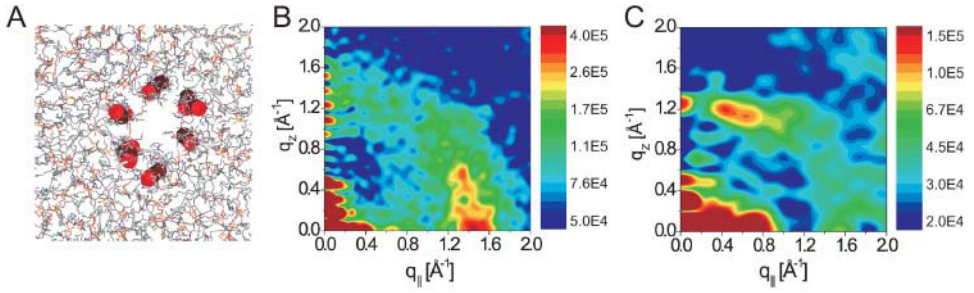

FIGURE 4 (*A*) The result of an MD simulation (Tieleman et al., 1999b) of an alamethicin pore in POPC with six peptides in top view. As in Fig. 1 the helix backbones are displayed as tubes. (*B* and *C*) The logarithmic plot of the structure factor of the whole coordinate set (without water molecules) and of only the alamethicin molecules, respectively.

to membrane-peptide interactions, e.g., due to hydrophobic matching. In this work, the helix peak of alamethicin in DLPC and OPPC membranes has been measured by reciprocal space mappings (RSMs) and is analyzed in view of the models presented in the previous section.

Fig. 5 shows the intensity distribution in form of two RSMs at different peptide/lipid concentrations of alamethicin in DLPC: at $P/L = 1{:}100$ (Fig. 5 *A*) and at $P/L = 1{:}10$ (Fig. 5 *B*), recorded at the D4 beamline. The results are quite unexpected and surprising: The addition of peptides leads to a strong novel scattering distribution which is distinctly different from the pure lipid. A pronounced circular arc appears at a radial distance of $\sim$1.4 Å^{-1} from the origin, which is not observed in the peptide-free case; see Spaar and Salditt (2003). Its intensity strongly increases with P/L. Even though very different from the expected pattern for transmembrane helices, we attribute this signal to the peptide helices, since its maximum is located near the q_z axis, in contrast to the chain correlation peak which is strongest at $q_z = 0$ and decreases for increasing angle to the $q_\parallel$ axis. At the same P/L, nothing unusual is observed in the reflectivity curves indicating that lamellar ordering is not destroyed and the principle bilayer structure (i.e., the orientational alignment of the membranes) is preserved (see Fig. 1, *b* and *c*). At $P/L = 1{:}10$ (Fig. 5 *B*) the helical scattering signal is stronger than the well-known acyl correlation peak which dominates the wide-angle scattering of pure lipid bilayers. Note, however, that from previous experiments we know that the chain correlation peak decreases in intensity with P/L indicating the loss of positional correlations of the lipid chains (frustrated packing) upon the insertion of transmembrane peptides (Münster et al., 2002). However, although samples containing magainin 2 only showed a weak helical peak, the signal is surprisingly clear and strong for alamethicin. The shape of the helical scattering differs significantly from the numerically computed structure factor of alamethicin in Fig. 3 *A*. In the following we interpret the circular shape of the peak by assuming a distribution of helix tilt angles with respect to the membrane normal. Note that the circular shape of the peak is attributed to a distribution of the peptide tilt angles and not to a distribution of orientation of the membrane normal itself (mosaicity). Based on this explanation, the helix parameters can be calculated as functions of the angle ϕ to the $q_\parallel$ axis from the position and the width of the peak in radial slices. Since the radial position of the peak maximum is nearly constant as a function of ϕ, we conclude that the helical pitch is approximately constant for different tilt angles. Radial slices through the intensity matrix at different angles ϕ to the $q_\parallel$ axis have been fitted to a Gaussian peak on a linear background.

To obtain the helical pitch from the peak maximum $q_0(\phi)$, the $q_\parallel$-value of the helix peak is needed in addition. We can assume a constant value of $q_{0,\parallel} = 0.64$ Å^{-1} from Fig. 3 *A*, assuming that the helix radius is constant under compression of the helix. In the coordinate system of the rotated helix, the corresponding value $q_{0,z}$ of the peak is then derived from $q_{0,z}(\phi) = \sqrt{q_0(\phi)^2 - q_{0,\parallel}}$. The pitch and helix length then follow from the approximations of the ideal helix, i.e., Eqs. 2 and 3. Note that this analysis is somewhat oversimplified leading to effective parameters which may indicate a general

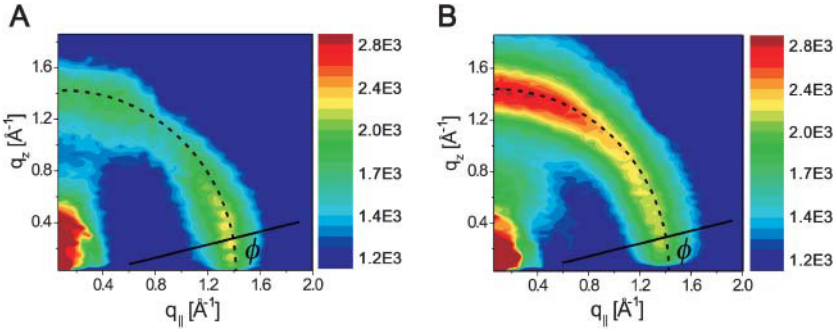

FIGURE 5 Diffraction patterns of (*A*) alamethicin in DLPC with $P/L = 1{:}100$ and (*B*) with $P/L = 1{:}10$, measured at the D4 beamline. The dashed line is a circle with a radius of 1.42 Å to indicate the position of the helix peak near the q_z axis.

trend, but may not accurately describe the helical structure. A modeling of the entire intensity distribution using a convolution over the tilt angle distribution would be more accurate. However, for the moment we stay within the framework of this simple model, before a simulation of the entire pattern is carried out further below. A further source of complication arises from the fact that the measured pattern contains both peptide and lipid contributions. In Fig. 6 the computed helix parameters P and the number of turns are displayed for angles, $\phi \geq 60°$ for $P/L = 1{:}100$ and $\phi \geq 30°$ for $P/L = 1{:}10$, over a range where the contribution of the lipid correlation peak is believed to be a minor effect. Note that the angle ϕ is uniquely related to the helix tilt angle χ, and that the measured pattern can only be explained on the basis of a broad distribution of angles χ, see also the form factor of the inserted (transmembrane) peptide ($\chi = 0°$), and the parallel adsorbed peptide ($\chi = 90°$), Fig. 3, *A* and *B*, respectively. The results thus indicate the following trend: The helix length or equivalently the number of turns increase for increasing ϕ, i.e., for decreasing helix tilt angle. At $P/L = 1{:}10$ the number of turns is ~0.8 higher than at $P/L = 1{:}100$. The helix pitch decreases for increasing ϕ at $P/L = 1{:}10$, whereas at $P/L = 1{:}100$ the behavior is not clear. Note that at $P/L = 1{:}100$ the error bar is larger because of the lower peak intensity. Therefore, we concentrate on the analysis of the $P/L = 1{:}10$ curve: The pitch of the peptides in transmembrane orientation, i.e., at $\chi \sim 0°$, is $P \simeq 4.95$ Å, and increases up to 5.1 Å for $\chi \sim 90°$. The helix length is ~18.3 Å at small tilt angle, and the number of helix turns is 3.7. This result is very plausible, since the alamethicin backbone roughly corresponds to a four-turn helix up to the Pro^{14} residue. Consequently, it suggests that approximately 10 residues are in helical conformation embedded in the hydrophobic region of the lipid chains. The results are in agreement with N-terminal insertion into the bilayer, with, however, a large angular distribution of tilt angles. The polar side groups of the helix can be expected to point to the hydrophilic headgroups.

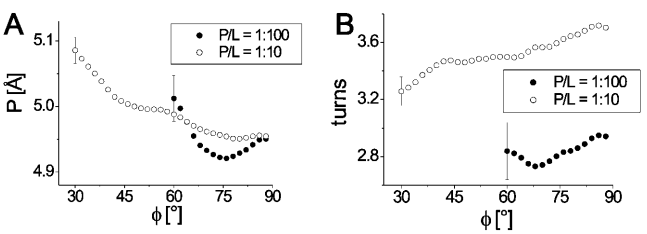

FIGURE 6 The results of the angular-dependent evaluation of the helix peak in Fig. 5, *A* and *B*, by Gaussian fits of radial slices. Displayed are (*A*) the helix pitch P and (*B*) the number of helical turns, as functions of the angle ϕ between the radial slices and the $q_{\|}$ axis in the RSMs. The pitch and the number of turns are shown for a range where the contribution of the lipid correlation peak is believed to be a minor effect. The error bars at $\phi = 60°$ for $P/L = 1{:}100$ and $\phi = 30°$ for $P/L = 1{:}10$ indicate the fluctuations of the values that stem from the fitting procedure.

Additional experiments were carried out on alamethicin at $P/L = 1{:}25$ in OPPC at the ID1 undulator beamline. The resulting RSM is displayed in Fig. 7 *A*, after combination of several CCD shots (leading to the sharp boundaries in the combined image). The helix peak is again clearly visible as a circular arc with a radius of $q \simeq 1.37$ Å^{-1} and a maximum at high angles ϕ. An evaluation of the angular dependence as in Fig. 6 is not possible, however, since the automated fitting routine often failed due to the sharp edges in the RSM. Therefore, we just show a cut through the helix peak (*circles*) at an angle of $\phi = 85°$ in the inset of Fig. 7 *A*, together with a fit (*solid line*) to a Gaussian curve on linear background. The peak center is at $q_0 = 1.37$ Å^{-1}, and the width is $\omega = 0.29$ Å^{-1} (FWHM). With the same assumption as in the previous evaluation of the RSM of alamethicin in DLPC, a helical pitch of 5.2 Å is obtained. From the peak width a helix length of 19.5 Å is determined, i.e., approximately four turns of the peptide helix are inserted into the lipid membranes. Again assuming N-terminal insertion of the peptide, this indicates an insertion up to the Pro^{14} residue. This result for OPPC is thus similar to DLPC, with a helical pitch P being somewhat larger. Again, since the proline acts as a bend in the peptide helix, the partial helical conformation is reasonable. The shape of the helix peak in the measured RSM is not exactly circular. For large ϕ the radius is about $q \simeq 1.37$ Å^{-1}, for smaller angles, $\phi \leq 45°$, and the peak center moves toward smaller q-values, down to $q \simeq 1.3$ Å^{-1}. This corresponds to a helical pitch of 5.6 Å, a value quite close to the pitch of 5.7 Å from the x-ray crystallography structure (Fox and Richards, 1982). The helix peak of alamethicin in OPPC can be therefore interpreted in such a way that the helical structure of parallel adsorbed peptides is close to structure from the Protein Data Bank, whereas a considerable fraction of the peptides is inserted up to the Pro^{14} residue. As obtained from reflectivity measurements, the PtP-distance of a pure OPPC membrane is ~37 Å, approximately twice the length of the inserted helix. The decrease of the helical pitch to 5.2 Å can therefore be understood as a matching of the inserted peptide helix to the thickness of one lipid layer.

As discussed above, it is not really clear whether the evaluation of the arc-shaped helix peak in terms of the two parameters, radial position and radial width, is appropriate. A more rigorous treatment of tilted peptides and peptide assemblies should quantify the distribution of helix tilt angles by comparison between simulated and experimental RSMs. As a first step toward this goal, we have extended the numerical structure factor analysis presented in Fig. 3, to reproduce more closely the experimentally observed helix peaks in Fig. 5 *A* and Fig. 7 *A*. Various combinations of the structure factors of alamethicin with different tilt angle have been evaluated, aiming at information about the angular distribution of the peptides. This analysis results in a Gaussian distribution of the tilt angles, with the center at $\chi = 0°$ (inserted state) and a width of 18° (half-width at half-maximum, i.e., HWHM). The modeled structure factor is

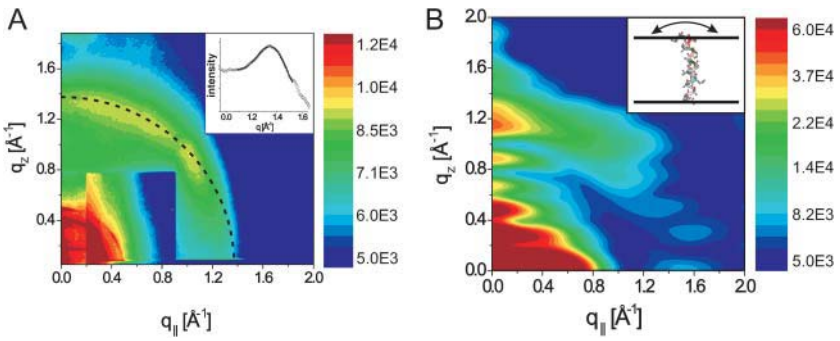

FIGURE 7 (*A*) Diffraction pattern of OPPC with alamethicin at $P/L = 1{:}25$, measured at the ID1 beamline. The dashed line is a circle with a radius of 1.37 $Å^{-1}$ to indicate the position of the helix peak near the q_z axis. In the inset a slice through the RSM data matrix at an angle $\phi = 85^{\circ}$ to the sample horizon (*circles*) and a Gaussian fit on linear background (*solid line*) are displayed. (*B*) The modeled structure factor of a Gaussian distribution of alamethicin tilt angles, with the center at $\chi = 0°$ (inserted state) and a width of 18° (HWHM). The superimposed helix peaks lead to a circular arc similar to the experimentally observed helix signal in *A* (this figure), and in Fig. 5 *A*.

shown in Fig. 7 *B*. Assuming this broad distribution of tilt angles, the superimposed helix peaks lead to a circular arc similar to the experimental observation, with the peak center located on the q_z axis. However, the comparison of this simulation to the experimental RSMs has to be considered with caution, since in the numerical computations the number of atoms is very small and finite size broadening is observed in the forward direction in the vicinity of the origin. Furthermore, some less-pronounced features in the simulation such as the side oscillations are expected to be smeared out, for example, by conformational fluctuations of the side chains.

SUMMARY AND CONCLUSIONS

In summary, we have shown that the helical scattering intensity can be measured in highly oriented membranes at signal/noise ratios sufficient for quantitative data analysis. Alamethicin leads to a particularly pronounced scattering pattern with a circular shape; the scattering intensity obviously increases with molar P/L. At high peptide concentrations it is stronger than the contribution of the lipid chain correlations, which decrease with P/L. A significant difference in the helical scattering of alamethicin and magainin 2 must be noted: Compared to recent experiments on magainin 2 in DMPC, the helix peak of alamethicin (measured here in DLPC and OPPC) is much stronger and smeared out on the circular arc, whereas it is rather weak but more localized in magainin (Münster et al., 2002). The strong intensity and circular arc observed here for alamethicin indicates that a predominant population of peptides is in the inserted (transmembrane) state with, however, a broad distribution of tilt angles with respect to the membrane normal. It has been proven that the circular shape cannot be interpreted as a misorientation of the membranes. The arc-like shape of the alamethicin peak was quantified by evaluating the helix parameters as a function of the helix tilt angle. The distribution of helix tilt angles was estimated by a numerical modeling of the helix peak. Surprisingly, the helical scattering intensity was stronger than the contribution of lipid acyl chains in the experiment with alamethicin in DLPC at $P/L = 1{:}10$. The peak width was found to be in agreement with a N-terminal insertion up to Pro^{14}, a residue which is known to destabilize the helix and that may induce a kink (hinge) in the molecule. The result of a rather continuous distribution of alamethicin tilt angles is in contrast to a pure two-state model (parallel, inserted) which may apply to magainin 2. The observed intensity distribution is also in contrast to the Fourier transform of the published coordinates of a MD simulation of six alamethicin molecules in a POPC bilayer. We therefore conclude that oligomeric pores at least of the specific type equilibrated in the MD study are not the predominant conformation. This configuration is probably not stable under the given experimental conditions (fluid L_α phase, $T = 40°C$, partial hydration). It is interesting to discuss the present results in view of the barrel stave-type oligomeric pores, as recorded by Huang and co-workers from in-plane neutron scattering studies. In principle, oligomeric pores can be reconciled with the present results if they leave enough conformational space of helical tilts and if they do not require the entire peptide to be inserted as in the MD study. In particular, an oligomeric pore constructed of a twinned set of partially inserted N-termini in both leaflets of the bilayer may seem possible. An alternative explanation would suggest isolated peptides with inserted helical segments starting at the N-terminus up to Pro^{14} similar to the MD study by La Rocca et al. (1999). In both cases, the helical segments would be characterized by a broad range of tilt angles. In the future, the influence of temperature T, hydration, P/L, and hydrophobic thickness of the lipid bilayer on the helical scattering distribution is to be investigated.

On the technical level, we have shown that the scattering distribution as measured by reciprocal space mappings (RSMs) can be compared to simple analytical expressions, as well as to numerical simulations starting from molecular coordinates of the Protein Data Bank, or alternatively published MD coordinates. For a single ideal helix, the helical pitch and the number of turns, or equivalently, the helix length can easily be calculated. The results of the ideal helix can then be generalized to oligomeric pores. Alternatively, models starting from atomic coordinates can be constructed. However, the conformation as obtained from x-ray crystallography must not necessarily apply to the

conformation of the peptide in or at the lipid bilayer. Although the obtained results are reasonable, the analytical evaluation and the numerical modeling of the helix scattering is still quite simplistic and relies on a number of assumptions. Furthermore, the scattering from the peptides is accompanied by the scattering of the surrounding lipid bilayer. It is therefore a clear advantage to compare the x-ray scattering results to the Fourier transform of MD simulation coordinates. In the future, simultaneous refinement of x-ray data evaluation and MD parameters may lead to a better understanding of lipid-peptide structure and interaction.

APPENDIX: STRUCTURE FACTOR OF AN IDEAL HELIX

For the calculation, the z axis is defined as the direction of the helix axis. The helix parameters are the number of atoms N_h, the radius R_h, the pitch P and the number of atoms per pitch n_p. The polar angle between two neighbored atoms projected on the x,y plane is then $\Delta\phi = 2\ \pi/n_p$, the shift along the helix axis is $\Delta h = P/n_p$ and the total helix length is $L_h = N_h\ P/n_p$. The coordinates of the helix atoms are

$$x_n = R_h \cos(n\Delta\phi), \quad y_n = R_h \sin(n\Delta\phi), \quad z_n = n\Delta h, \quad \text{for } n = 1, \ldots, N_h. \tag{7}$$

The structure factor of a given coordinate set is calculated by

$$F_{helix}(q_\parallel, q_z) = \frac{1}{2\pi N_h} \int_0^{2\pi} d\varphi \times \left| \sum_{n=1}^{N_h} e^{i(q_\parallel (x_n \cos\varphi + y_n \sin\varphi) + q_z z_n)} \right|^2. \tag{8}$$

With the atomic positions in Eq. 7 and the interchange of the sum and the integral it can be written as

$$F_{helix}(q_\parallel, q_z) = \frac{1}{2\pi N_h} \sum_{m,n=1}^{N_h} e^{iq_z(m-n)P/n_p} \times \int_0^{2\pi} d\varphi\, e^{2iq_\parallel R_h \sin((m-n)\pi/n_p)\cos\varphi}. \tag{9}$$

The integral can be solved with the Bessel function J_0 (Gradshteyn and Ryzhik, 2000),

$$2\pi J_0(z) = \int_0^{2\pi} d\varphi\, e^{iz\cos\varphi}. \tag{10}$$

The structure factor is then expressed as a sum over the interatomic distances instead of a double sum over the atomic positions as

$$F_{helix}(q_\parallel, q_z) = 1 + 2 \sum_{\Delta n=1}^{N_h - 1} \left(1 - \frac{\Delta n}{N_h}\right) \times \cos\frac{q_z \Delta n P}{n_p} J_0\left(2\, q_\parallel R_h \sin\frac{\Delta n \pi}{n_p}\right). \tag{11}$$

From this formula (Eq. 1 in the text) the position of the helix peak is derived as

$$q_\parallel = \frac{5\pi}{8R_h}, \quad q_z = \frac{2\pi}{P}. \tag{12}$$

To calculate the peak width along q_z, we use the structure factor of a one-dimensional lattice consisting of N atoms with a lattice constant d,

$$S(q_z) = \left| \frac{1}{N} \sum_{n=1}^{N} N e^{inq_z d} \right|^2, \tag{13}$$

which is identical to the form factor of a helix in Eq. 8 in the limit $R_h \to 0$. The geometric series can be evaluated as

$$S(q_z) = \frac{1}{N^2} \left| \frac{e^{iNq_z d} - 1}{1 - e^{-iq_z d}} \right|^2 = \frac{1}{N^2} \frac{1 - \cos(Nq_z d)}{1 - \cos(q_z d)} = \frac{1}{N^2} \frac{\sin^2(Nq_z d/2)}{\sin^2(q_z d/2)}. \tag{14}$$

This is the well-known expression for the Laue function or lattice structure factor.

The maximum amplitude of the structure factor is $S(q_z = 0) = 1$; the peak width ω (HWHM) is therefore defined by

$$S(q_z = \omega) = \frac{1}{2} \quad \rightarrow \quad \sin\frac{N\omega d}{2} = \frac{N}{\sqrt{2}} \sin\frac{\omega d}{2}. \tag{15}$$

With the definition of the dimensionless variable $a = N\omega\ d/2$ and the approximation of the sine function for large $N \gg 1$ the above equation can transformed to

$$\sin a = \frac{N}{\sqrt{2}} \sin\frac{a}{N} \simeq \frac{N}{\sqrt{2}} \frac{a}{N} = \frac{a}{\sqrt{2}}. \tag{16}$$

The resulting transcendental equation $\sin a = a/\sqrt{2}$ contains only the parameter a; the outcome of a numerical computation is $a = 1.3915575$. The peak width therefore can be written in terms of the number of atoms N and lattice constant d as

$$\omega \simeq \frac{5.57}{Nd} \quad \text{(HWHM)}. \tag{17}$$

The derived relation (Eq. 17) between the peak width and the lattice parameters N and d is quite universal, and in the text it is applied to obtain the number of helical turns from the width of the helix peak in Eq. 3.

We thank the European Synchrotron Radiation Source in Grenoble, France, for providing beamtime at the ID1 experimental station, and David Le Bolloch and Chenghao Li for help with the experiment.

Financial aid by the Deutsche Forschungsgemeinschaft through grants SA 772/3 and SA-772/4, and by the Federal Ministry of Research under grant number 05KS1TSA/7, is gratefully acknowledged.

REFERENCES

Aguilella, V. M., and S. M. Bezrukov. 2001. Alamethicin channel conductance modified by lipid charge. *Eur. Biophys. J.* 30:233–241.

Bak, M., R. P. Bywater, M. Hohwy, J. K. Thomsen, K. Adelhorst, H. J. Jakobsen, O. W. Sørensen, and N. C. Nielsen. 2001. Conformation of alamethicin in oriented phospholipid bilayers determined by ^{15}N solid state nuclear magnetic resonance. *Biophys. J.* 81:1684–1698.

Baumann, G., and P. Mueller. 1974. A molecular model of membrane excitability. *J. Supramol. Struct.* 2:538–557.

Bechinger, B. 1997. Structure and functions of channel-forming peptides: magainins, cecropins, melittin and alamethicin. *J. Membr. Biol.* 156:197–211.

Bechinger, B. 1999. The structure, dynamics and orientation of antimicrobial peptides in membranes by multidimensional solid-state NMR spectroscopy. *Biochim. Biophys. Acta.* 1462:157–183.

Biggin, P. C., J. Breed, H. S. Son, and M. S. Sansom. 1997. Simulation studies of alamethicin-bilayer interactions. *Biophys. J.* 72:627–636.

Biggin, P. C., and M. S. P. Sansom. 1999. Interactions of α-helices with lipid bilayers: a review of simulation studies. *Biophys. Chem.* 76: 161–183.

Boheim, G. 1974. Statistical analysis of alamethicin channels in black lipid membranes. *J. Membr. Biol.* 19:277–303.

Boheim, G., W. Hanke, and G. Jung. 1983. Alamethicin pore formation: voltage-dependent flip-flop of α-helix dipoles. *Biophys. Struct. Mech.* 9:181–191.

Bven, L., O. Helluin, G. Molle, H. Duclohier, and H. Wrblewski. 1999. Correlation between anti-bacterial activity and pore sizes of two classes of voltage-dependent channel-forming peptides. *Biochim. Biophys. Acta.* 1421:53–63.

Cafiso, D. S. 1994. Alamethicin: a peptide model for voltage gating and protein-membrane interactions. *Annu. Rev. Biophys. Biomol. Struct.* 23:141–165.

Cantor, R. S. 2002. Size distribution of barrel-stave aggregates of membrane peptides: influence of the bilayer lateral pressure profile. *Biophys. J.* 82:2520–2525.

Duclohier, H., and H. Wrblewski. 2001. Voltage-dependent pore formation and antimicrobial activity by alamethicin and analogues. *J. Membr. Biol.* 184:1–12.

Ehrenstein, G., and H. Lecar. 1977. Electrically gated ionic channels in lipid bilayers. *Q. Rev. Biophys.* 10:1–34.

Fox, R. O., Jr., and F. M. Richards. 1982. A voltage-gated ion channel model inferred from the crystal structure of alamethicin at 1.5-Å resolution. *Nature.* 300:325–330.

Galaktionov, S. G., and G. R. Marshall. 1993. Effects of electric field on alamethicin bound at the lipid-water interface: a molecular mechanics study. *Biophys. J.* 65:608–617.

Gradshteyn, I. S., and I. M. Ryzhik. 2000. Table of Integrals, Series, and Products, 6th Ed. Academic Press, San Diego, CA.

Hall, J. E. 1981. Voltage-dependent lipid flip-flop induced by alamethicin. *Biophys. J.* 33:373–381.

He, K., S. J. Ludtke, W. T. Heller, and H. W. Huang. 1996a. Mechanism of alamethicin insertion into lipid bilayers. *Biophys. J.* 71:2669–2679.

He, K., S. J. Ludtke, D. L. Worcester, and H. W. Huang. 1996b. Neutron scattering in the plane of membranes: structure of alamethicin pores. *Biophys. J.* 70:2659–2666.

Huang, H. W. 2000. Action of antimicrobial peptides: two-state model. *Biochemistry.* 39:8347–8352.

Ionov, R., A. El-Abed, A. Angelova, M. Goldmann, and P. Peretti. 2000. Asymmetrical ion-channel model inferred from two-dimensional crystallization of a peptide antibiotic. *Biophys. J.* 78:3026–3035.

Jayasinghe, S., M. Barrenger-Mathys, J. F. Ellena, C. Franklin, and D. S. Cafiso. 1998. Structural features that modulate the transmembrane migration of a hydrophobic peptide in lipid vesicles. *Biophys. J.* 74: 3023–3030.

Katsaras, J., R. S. Prosser, R. H. Stinson, and J. H. Davis. 1992. Constant helical pitch of the gramicidin channel in phospholipid bilayers. *Biophys. J.* 61:827–830.

Kessel, A., and N. Ben-Tal. 2002. Energetics of peptide-membrane systems. *In* Current Topics In Membranes. S. A. Simon, and T. J. McIntosh, editors. Academic Press.

Kessel, A., D. S. Cafiso, and N. Ben-Tal. 2000a. Continuum solvent model calculations of alamethicin-membrane interactions: thermodynamic aspects. *Biophys. J.* 78:571–583.

Kessel, A., K. Schulten, and N. Ben-Tal. 2000b. Calculations suggest a pathway for the transverse diffusion of a hydrophobic peptide across a lipid bilayer. *Biophys. J.* 79:2322–2330.

La Rocca, P., P. C. Biggin, D. P. Tieleman, and M. S. P. Sansom. 1999. Simulation studies of the interaction of antimicrobial peptides and lipid bilayers. *Biochim. Biophys. Acta.* 1462:185–200.

Ludtke, S. J., K. He, W. T. Heller, T. A. Harroun, L. Yang, and H. W. Huang. 1996. Membrane pores induced by magainin. *Biochemistry.* 35:13723–13728.

Marsh, D. 1996. Peptide models for membrane channels. *Biochem. J.* 315:345–361.

Matsuzaki, K. 1998. Magainins as paradigm for the mode of action of pore forming polypeptides. *Biochim. Biophys. Acta.* 1376:391–400.

Matsuzaki, K. 1999. Why and how are peptide-lipid interactions utilized for self-defense? Magainins and tachyplesins as archetypes. *Biochim. Biophys. Acta.* 1462:1–10.

Mennicke, U., and T. Salditt. 2002. Preparation of solid-supported lipid bilayers by spin-coating. *Langmuir.* 18:8172–8177.

Müller, J., C. Münster, and T. Salditt. 2000. Thermal denaturing of bacteriorhodopsin by x-ray scattering from oriented purple membranes. *Biophys. J.* 78:3208–3217.

Münster, C., A. Spaar, B. Bechinger, and T. Salditt. 2002. Magainin 2 in phospholipid bilayers: peptide orientation and lipid chain ordering studied by x-ray diffraction. *Biochim. Biophys. Acta.* 1562:37–44.

Nagle, J. F., and J. Katsaras. 1999. Absence of a vestigial vapor pressure paradox. *Phys. Rev. E.* 59:7018–7024.

Pauling, L., and R. B. Corey. 1951. Atomic coordinates and structure factors for two helical configurations of polypeptide chains. *Proc. Natl. Acad. Sci. USA.* 37:235–240.

Podgornik, R., and V. A. Parsegian. 1997. On a possible microscopic mechanism underlying the vapor pressure paradox. *Biophys. J.* 72:942–952.

Salditt, T., T. H. Metzger, J. Peisl, and G. Goerigk. 1995. Nonspecular x-ray scattering from thin films and multilayers with the small-angle scattering equipment. *J. Phys. D.* 28:A236–239.

Sansom, M. S. P. 1993. Alamethicin and related peptaibols—model ion channels. *Eur. Biophys. J.* 22:105–124.

Schwarz, G., and P. Savko. 1982. Structural and dipolar properties of the voltage-dependent pore former alamethicin in octanol/dioxane. *Biophys. J.* 39:211–219.

Seul, M., and M. J. Sammon. 1990. Preparation of surfactant multilayer films on solid substrates by deposition from organic solution. *Thin Solid Films.* 185:287–305.

Shai, Y. 1999. Mechanism of the binding, insertion and destabilization of phospholipid bilayer membranes by α-helical antimicrobial and cell non-selective membrane-lytic peptides. *Biochim. Biophys. Acta.* 1462:55–70.

Sitaram, N., and R. Nagaraj. 1999. Interaction of antimicrobial peptides with biological and model membranes: structural and charge requirements for activity. *Biochim. Biophys. Acta.* 1462:29–54.

Spaar, A., and T. Salditt. 2003. Short range order of hydrocarbon chains in fluid phospholipid bilayers studied by x-ray diffraction from highly oriented membranes. *Biophys. J.* 85:1576–1584.

Tieleman, D. P., H. J. C. Berendsen, and M. S. P. Sansom. 1999a. An alamethicin channel in a lipid bilayer: molecular dynamics simulations. *Biophys. J.* 76:1757–1769.

Tieleman, D. P., H. J. C. Berendsen, and M. S. P. Sansom. 1999b. Surface binding of alamethicin stabilizes its helical structure: molecular dynamics simulations. *Biophys. J.* 76:3186–3191.

Tieleman, D. P., H. J. C. Berendsen, and M. S. P. Sansom. 2001. Voltage-dependent insertion of alamethicin at phospholipid/water and octane/water interfaces. *Biophys. J.* 80:331–346.

Tieleman, D. P., B. Hess, and M. S. P. Sansom. 2002. Analysis and evaluation of channel models: simulations of alamethicin. *Biophys. J.* 83:2393–2407.

Tieleman, D. P., M. S. P. Sansom, and H. J. C. Berendsen. 1999c. Alamethicin helices in a bilayer and in solution: molecular dynamics simulations. *Biophys. J.* 76:40–49.

Vodyanoy, I., J. E. Hall, and T. M. Balasubramanian. 1983. Alamethicin-induced current-voltage curve asymmetry in lipid bilayers. *Biophys. J.* 42:71–82.

Woolley, G. A., P. C. Biggin, A. Schultz, L. Lien, D. C. J. Jaikaran, J. Breed, K. Crowhurst, and M. S. P. Sansom. 1997. Intrinsic rectification of ion flux in alamethicin channels: studies with an alamethicin dimer. *Biophys. J.* 73:770–778.

Woolley, G. A., and B. A. Wallace. 1993. Temperature dependence of the interaction of alamethicin helices in membranes. *Biochemistry.* 32:9819–9825.

Yang, L., T. M. Weiss, T. A. Harroun, W. T. Heller, and H. W. Huang. 1999. Supramolecular structures of peptide assemblies in membranes by neutron off-plane scattering: method of analysis. *Biophys. J.* 77:2648–2656.

Yang, L., T. M. Weiss, R. I. Lehrer, and H. W. Huang. 2000. Crystallization of antimicrobial pores in membranes: magainin and protegrin. *Biophys. J.* 79:2002–2009.

Yee, A. A., K. Marat, and J. D. J. O'Neil. 1997. The interactions with solvent, heat stability, and ^{13}C-labelling of alamethicin, an ion-channel-forming peptide. *Eur. J. Biochem.* 243:283–291.